

# Temporally versatile polarization entanglement from Bragg-reflection waveguides

A. Schlager,<sup>1</sup> B. Pressl,<sup>1</sup> K. Laiho,<sup>1,\*</sup> H. suchomel,<sup>2</sup> M. Kamp,<sup>2</sup> S. Höfling,<sup>2,3</sup> C. Schneider,<sup>2</sup> and G. Weihs<sup>1</sup>

<sup>1</sup>*Institut für Experimentalphysik, Universität Innsbruck, Technikerstraße 25, 6020 Innsbruck, Austria*

<sup>2</sup>*Technische Physik, Universität Würzburg, Am Hubland, 97074 Würzburg, Germany*

<sup>3</sup>*School of Physics & Astronomy, University of St Andrews, St Andrews, KY16 9SS, United Kingdom*

Bragg-reflection waveguides emitting broadband parametric down-conversion (PDC) have been proven to be well suited for the on-chip generation of polarization entanglement in a straightforward fashion [R. T. Horn et al., *Sci. Rep.* 3, 2314 (2013)]. Here, we investigate how the properties of the created states can be modified by controlling the temporal delay between the pair of photons created via PDC. Our results offer an easily accessible approach for changing the coherence of the polarization entanglement, in other words, to tune the phase of the off-diagonal elements of the density matrix. Furthermore, we provide valuable insight in the engineering of these states directly at the source.

The verification of the non-classical nature of quantum objects, such as photons, plays an important role to ensure a successful implementation of forthcoming quantum technologies. Among these tasks is the preparation and characterization of polarization entanglement that provides some of the strongest evidence of the quantum features of light [1–3]. Since the first realizations with parametric down-conversion (PDC) in bulk crystals more than two decades ago [4–6], a lot of effort has been put in replacing them both with ferroelectric [7–11] and semiconductor waveguides [12–14], which provide higher brightnesses and easier alignment in collinear configurations.

In one of such configurations, the cross-polarized PDC photon pairs—called signal and idler—that have at least some nanometers of spectral extent, are divided on a dichroic beam splitter into two paths [15–19]. Due to the strict frequency *or* energy correlation between them, a two-partite superposition is created between the output paths of the dichroic mirror. Often, a continuous-wave pump laser is utilized to guarantee tight correlations in the spectral domain [14, 20]. This way the spectral overlap of signal and idler is optimized, and thus also the polarization entanglement.

In comparison to the traditional birefringent crystals and waveguides, Bragg-reflection waveguides (BRWs) generate indistinguishable photon pairs over several tens of nanometers [14, 21] and they have been utilized for narrowband multiplexing of polarization entanglement [22, 23]. Due to the very small birefringence between the orthogonally-polarized signal and idler [24], BRWs work in the used configurations even without delay compensation. However, their group index difference is large enough to result into an uncontrolled phase. Therefore, the engineering of the spectro-temporal degree of freedom of PDC photon pairs from BRWs is essential for the controlled creation and manipulation of the polarization entanglement.

Changes in the coherence of the polarization entangled states, that is their phase, provide an interesting

degree of freedom for the state manipulation [2]. When regarding PDC sources, this is usually accomplished by modifying the characteristics of one of the entangled parties with birefringent retarders [14, 25, 26]. However, the phase control over the joint state can possibly be realized more easily [27–29]. Here, we generate broadband, pulsed polarization entanglement from a collinear BRW source emitting PDC. As the intrinsic group delay of signal and idler causes an uncontrolled phase, we tailor the coherence of the created state by introducing an optical path length difference for them. Our results show that the phase of the created state can be tuned flexibly in a very simple manner. Further, we provide an important insight into how the spectro-temporal properties of the joint PDC state can be taken advantage of in the creation of polarization entanglement.

Our BRW source generates cross-polarized signal and idler photons via a type-II PDC process. In the low gain regime, the photon-pair state can be approximated as [30, 31]

$$|\psi\rangle = \iint d\omega_s d\omega_i f(\omega_s, \omega_i) \hat{a}_H^\dagger(\omega_s) \hat{a}_V^\dagger(\omega_i) |0\rangle, \quad (1)$$

in which  $f(\omega_s, \omega_i)$  describes the joint spectral amplitude (JSA) of signal ( $s$ ) and idler ( $i$ ) in terms of their frequencies  $\omega_\mu$  ( $\mu = s, i$ ). The operator  $\hat{a}_\sigma^\dagger(\omega)$  accounts for the creation of a photon with a specific frequency at either horizontal ( $H$ ) or vertical ( $V$ ) polarization ( $\sigma = H, V$ ). The normalization condition ensures that  $\iint d\omega_s d\omega_i |f(\omega_s, \omega_i)|^2 = 1$ .

For the creation of polarization entanglement we employ the scheme illustrated in Fig. 1(a), also used with BRWs in Refs [14, 20]. The state from (1) is split at a dichroic mirror, which we model as a frequency dependent beam splitter. We take into account the finite transition bandwidth of the dichroic beam splitter and its polarization dependent behavior. Prior to that, the signal beam is delayed by a time  $\tau$  with respect to the idler. Thus, we apply the beam splitter transformations

$$\begin{aligned} \hat{a}_H^\dagger(\omega_s) &= \left[ \sqrt{T_H(\omega_s)} \hat{A}_H^\dagger(\omega_s) - \sqrt{R_H(\omega_s)} \hat{B}_H^\dagger(\omega_s) \right] e^{-i\omega_s \tau} \quad \text{and} \\ \hat{a}_V^\dagger(\omega_i) &= \sqrt{T_V(\omega_i)} \hat{A}_V^\dagger(\omega_i) - \sqrt{R_V(\omega_i)} \hat{B}_V^\dagger(\omega_i), \end{aligned} \quad (2)$$

\* [kaisa.laiho@uibk.ac.at](mailto:kaisa.laiho@uibk.ac.at)

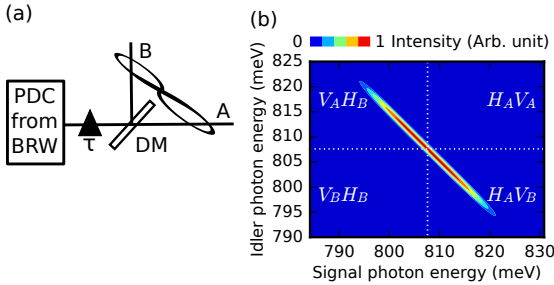


FIG. 1. (a) Scheme for creating polarization entangled states via the type-II PDC emission from a BRW, in which signal and idler pass a polarization selective delay of  $\tau$  before being split at a dichroic mirror (DM) into two paths  $A$  and  $B$ . (b) The absolute value of the simulated JSA of our BRW subjected to the spectral filtering of our experiment. It is calculated using the PDC process parameters measured in Refs [24, 32]. The output paths taken by the  $H$ -polarized signal and  $V$ -polarized idler are shown in the different spectral regions. The dotted lines mark the central wavelength of a narrowband DM.

in which  $T_\sigma(\omega_\mu)$  and  $R_\sigma(\omega_\mu)$  are the frequency and polarization dependent real-valued transmission and reflection coefficients of the dichroic mirror, for which the relation  $T_\sigma(\omega_\mu) + R_\sigma(\omega_\mu) = 1$  holds. Further, in (2) the properties of signal and idler are expressed in terms of the transmitted and reflected output arms of the dichroic mirror labeled with  $A$  and  $B$ , respectively.

We plug the transformations in (2) into (1) in order to derive the polarization entangled state. We keep only the terms that can cause coincidences between  $A$  and  $B$ . This approximation is justified by the shape of the JSA in our BRW and only a very small part of the JSA is neglected as illustrated in Fig. 1(b). We express the post-selected state in the form

$$|\phi\rangle \approx \iint d\omega_s d\omega_i e^{-i\omega_s\tau} \left[ g(\omega_s, \omega_i) | \omega_s, H \rangle_A | \omega_i, V \rangle_B + h(\omega_s, \omega_i) | \omega_i, V \rangle_A | \omega_s, H \rangle_B \right], \quad (3)$$

in which

$$g(\omega_s, \omega_i) = f(\omega_s, \omega_i) \sqrt{T_H(\omega_s) R_V(\omega_i)} \quad \text{and} \quad (4)$$

$$h(\omega_s, \omega_i) = f(\omega_s, \omega_i) \sqrt{R_H(\omega_s) T_V(\omega_i)}. \quad (5)$$

Further, we use the short notation  $\hat{A}_\sigma^\dagger(\omega_\mu) |0\rangle = |\omega_\mu, \sigma\rangle_A$  and similar for the arm  $B$  in (3).

In order to calculate the density matrix of the polarization entangled state  $\rho$  we trace the density matrix  $\tilde{\rho} = |\phi\rangle\langle\phi|$  of the state in (3) over the signal and idler frequencies and obtain

$$\rho = 1/\mathcal{N} \iint d\omega' d\omega'' A \langle \omega' | B \langle \omega'' | \tilde{\rho} | \omega'' \rangle_B | \omega' \rangle_A, \quad (6)$$

in which  $\mathcal{N}$  is a normalization constant. Using the relation  $A \langle \omega' | \omega_\mu, \sigma \rangle_A = \delta(\omega' - \omega_\mu) |\sigma\rangle_A$  and similar for the arm  $B$ , we can rewrite the density matrix of the polarization entangled state in (6) as

$$\rho = \alpha |HV\rangle_{AB} \langle HV| + \mathcal{D}(\tau) |VH\rangle_{AB} \langle VH| + \mathcal{D}^*(\tau) |HV\rangle_{AB} \langle VH| + \beta |VH\rangle_{AB} \langle VH| \quad (7)$$

in which  $\alpha$  and  $\beta$  are the diagonal elements of the density matrix, the sum of which is normalized to unity. The complex-valued off-diagonal elements,  $\mathcal{D}(\tau)$  and its complex conjugate  $\mathcal{D}^*(\tau)$ , quantify the amount of entanglement in the created state, which we call the *degree of polarization entanglement*, shortly  $\mathcal{D}$ -parameter [33]. This parameter is highly dependent on  $\tau$  and the state characteristics can be manipulated by changing the delay between signal and idler.

The elements of the density matrix in (7) are determined by the spectral properties of the PDC emission and can be evaluated via  $\alpha = 1/\mathcal{N} \iint d\omega' d\omega'' |g(\omega', \omega'')|^2$ ,  $\beta = 1/\mathcal{N} \iint d\omega' d\omega'' |h(\omega'', \omega')|^2$  as well as

$$\mathcal{D}(\tau) = 1/\mathcal{N} \iint d\omega' d\omega'' e^{i(\omega' - \omega'')\tau} h(\omega'', \omega') g^*(\omega' \omega''). \quad (8)$$

We emphasize that the trace over the frequencies in (6) causes mixedness and therefore, the density matrix cannot generally be written in terms of a pure polarization entangled state. Moreover, the purity of the state in (7) is greatly dependent on the temporal characteristics of the  $\mathcal{D}$ -parameter that are governed by the properties of the underlying PDC process [33–35].

In our experiment shown in Fig. 2 we use a pulsed laser as the pump of the PDC process, whose spectral properties (767.6 nm central wavelength, 0.8 nm bandwidth) are controlled with a grating setup. After spatial mode control with a single mode fiber, the proper power and polarization of the pump beam are chosen. The pump pulses are coupled into our BRW with a 100x microscope objective and collimated afterwards with a high numerical aperture aspheric lens having a 3 mm focal length.

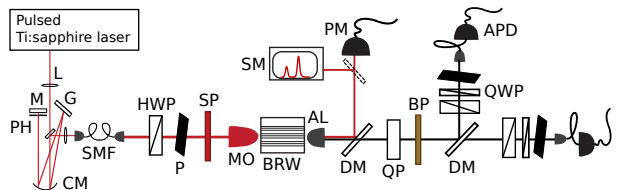


FIG. 2. Setup for creating and characterizing the polarization entanglement from a BRW. Abbreviations: AL = aspheric lens, APD = avalanche photo-diode, BP = band pass filter, CM = curved mirror, DM = dichroic mirror, G = grating, HWP = half-wave plate, L = lens, M = mirror, MO = microscope objective, P = polarizer, PH = pinhole, PM = power meter, QP = quartz plate, QWP = quarter-wave plate, SM = spectrometer, SMF = single mode fiber, SP = short pass filter.

The investigated BRW with 4  $\mu\text{m}$  ridge width is 1.87 mm long and its front facet is anti-reflection coated for the pump wavelengths. Behind the BRW, the pump beam with an average power of about 250  $\mu\text{W}$  is separated from the emitted signal and idler beams with a dichroic mirror. Thereafter, a spectral filter with 40 nm bandwidth and a central wavelength of 1535.2 nm, corresponding to the PDC degeneracy wavelength, is employed to limit the spectral extent of the emitted photon pairs in order to guarantee good spectral overlap between them. The PDC emission is then sent to a dichroic mirror centered at the degeneracy and having about 7 nm broad step between transmission and reflection bands for the both polarizations. At the two output arms we use a combination of half- and quarter-wave plates as well as sheet polarizers for setting the desired polarizations for the tomographic reconstruction of the density matrix. Finally, we couple the transmitted light into single mode fibers and use commercial, gated avalanche photo-detectors having a quantum efficiency of about 0.2 for counting the coincidences and singles at a measurement rate of 1.9 MHz and acquisition time of 2 min.

The pump power of our BRW source is set such that the coincidences-to-accidentals ratio (CAR) is 9.5(5). A high value of the CAR is desired in order to suppress the higher photon-number contributions in the PDC emission that otherwise cause an undesired background on the measured coincidences. It is also a strong evidence of simultaneous production of photons in signal and idler beams, i.e. the pair production.

We implement a temporal delay between signal and idler with a 0.82 mm thick quartz plate, which according to our earlier experiments [24] is necessary for compensating the group delay between signal and idler. We verify the path length difference along the retarder's fast and slow axis with the help of a spectrophotometer having a spectral range of 0.5 – 2  $\mu\text{m}$  (Perkin-Elmer, Lambda 19). We place the retarder between two crossed polarizers such that the input polarization is rotated in the retarder due to its birefringence. The strong wavelength dependence of the retardance causes fringes in the system's transmission. This approach yields a temporal difference of  $\Delta\tau = 25.9(4)$  fs between its fast and slow axis near 1550 nm.

We reconstruct the density matrices of the generated states from 36 correlation measurements between the two output paths of the dichroic mirror. The created state is projected onto all polarization combinations of  $H/V$ ,  $D/A = (H \pm V)/\sqrt{2}$  and  $R/L = (H \pm iV)/\sqrt{2}$ . For the state tomography we employ standard optimization algorithms [36]. We further note that the selected polarizations fit well for signal and idler at the central wavelengths of the transmitted and reflected arms of the dichroic mirror. Although achromatic components are used, a polarimeter study reveals small deviations at the edges of these spectral bands from the desired polarizations.

The time delay between signal and idler is controlled

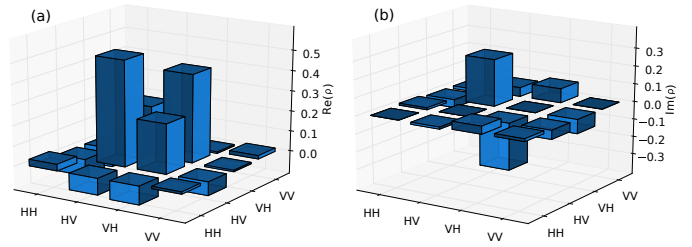


FIG. 3. (a) Real and (b) imaginary part of the reconstructed density matrix for the case (i). The two main diagonal elements of the density matrix take the values of 0.52(1) and 0.43(1). The undesired background in the remaining diagonal elements is about 0.05. The  $\mathcal{D}$ -parameter takes the value of  $0.244(13) \pm i \cdot 0.260(13)$  corresponding to the weights of the main off-diagonal elements.

with the orientation of the fast axis of the quartz plate or by removing it from the setup. In total we can measure the density matrix at three temporal delays of (i) 0, (ii)  $+\Delta\tau$  and (iii)  $-\Delta\tau$ . In Fig. 3 we show the reconstructed density matrix for the case (i). We clearly notice that the main diagonal elements of the density matrices have slightly different weights that can be explained by the asymmetry of the JSA, that is, the central wavelengths of the used broadband filter and the dichroic mirror were slightly mismatched. We further notice that due to spurious counts, there is a rather large background noise in many elements, most probably caused by the rather low CAR and other background light such as fluorescence from the BRW as well as imperfect optics distorting the desired polarization. However, most importantly, we see that the  $\mathcal{D}$ -parameter exhibits both real and imaginary parts, which means that the intrinsic group delay of signal and idler is non-negligible and causes an uncontrolled phase.

Next, we use the quartz plate to manipulate the  $\mathcal{D}$ -parameter, whereas the diagonal elements of the density matrix vary only slightly. In case (ii) we compensate the temporal delay between signal and idler to suppress the imaginary part of the off-diagonal terms in the density matrix. From the raw coincidence counts we extract the maximal visibilities of 0.78(3), 0.68(3) and 0.68(3) in H/V, A/D and R/L basis, respectively. We achieve a  $\mathcal{D}$ -parameter with the value of  $0.362(12) \pm i \cdot 0.133(13)$ . This parameter can also become fully imaginary close to the delay used in case (iii), in which case we extract the value of  $0.097(15) \pm i \cdot 0.244(15)$ . In order to examine this strong time-dependence in more detail, we illustrate in Fig. 4(a) the obtained  $\mathcal{D}$ -parameters with respect to the temporal delay between signal and idler together with the theoretical prediction from (8), which is calculated with the JSA from Fig. 1(b). The inset shows the purity of the created state with respect to the temporal delay, indicating a strong drop in it within the investigated time window. Further, in Fig. 4(b) we extract the phase of the  $\mathcal{D}$ -parameter, which exhibits a rather linear behavior.

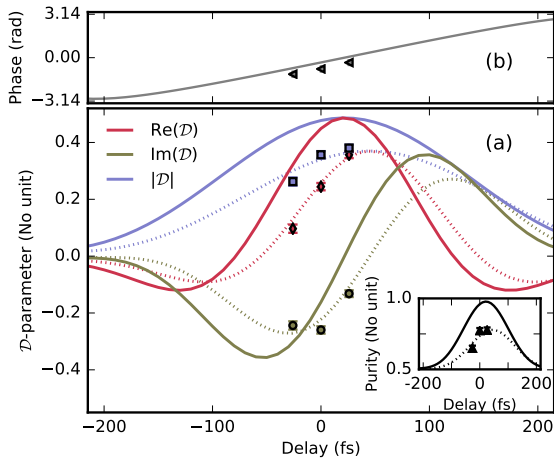


FIG. 4. (a) Predicted values for the real and imaginary parts as well as for the absolute value of the  $\mathcal{D}$ -parameter vs. the temporal delay. The measured values are marked with diamonds, circles and squares, respectively. The dotted lines illustrate the corresponding degradation of the theoretical curves due to the experimental imperfections. The inset shows the expected (solid line), due to the imperfections degraded (dotted line) and measured (symbols) purity extracted via  $\text{Tr}(\rho^2)$ . (b) The predicted phase (solid line) extracted via  $\arg(\mathcal{D})$  vs. the temporal delay together with the measured values (symbols).

The highest values for the  $\mathcal{D}$ -parameter and purity are reached as expected when the temporal delay between signal and idler is compensated, and the degree of polarization entanglement should be real-valued. Otherwise the state is mixed, finally exhibiting no coherence, in other words, the off-diagonal elements of the density matrix vanish. Nevertheless, within this time window we can tune the phase of the  $\mathcal{D}$ -parameter by changing the delay between signal and idler. Our theoretical predictions can qualitatively verify the expected trend, however, the measured values are somewhat decreased. First, we no-

tice from Fig. 4(b) that there is a remaining offset in the temporal delay. Second, the measured raw visibilities indicate that the amplitude of the  $\mathcal{D}$ -parameter is diminished due to spurious counts. After taking into account these two imperfections we find a good agreement with the theory and experiment also shown in Fig. 4(a). To summarize, we list the achieved values for the purity, fidelity and concurrence [37] in Table I.

Case	Purity	Fidelity	Concurrence
(i)	0.80(2)	93.2(6)	75(3)
(ii)	0.77(2)	93.0(6)	70(3)
(iii)	0.65(2)	92.3(7)	51(3)

TABLE I. Extracted values for the purity, fidelity with the simulated states from (7) evaluated via  $\text{Tr}(\sqrt{\rho^{1/2}\rho_{\text{Exp}}\rho^{1/2}})$  with  $\rho_{\text{Exp}}$  being the experimentally reconstructed density matrix, and concurrence for the cases (i)-(iii).

To conclude, we studied the temporal characteristics of the polarization entangled states in terms of the  $\mathcal{D}$ -parameter. These states were created by splitting the broadband, pulsed PDC emission from our BRW with a dichroic mirror and by manipulating the delay between signal and idler prior to that. Our results illustrate the necessity of an accurate temporal control when creating these states via PDC emitted from BRWs. We have shown that the group delay difference between signal and idler is non-negligible, affecting the  $\mathcal{D}$ -parameter in an uncontrolled manner. However, its phase can easily be tuned if the delay between signal and idler is changed, excluding the need for modifying the state afterwards in the individual paths of the two separate parties. Our results deliver insight into the internal phase of the PDC emission and emphasizes the possibilities for the state manipulation directly at the source.

This work was supported by the FWF through project no. I-2065-N27, the DFG Project no. SCHA1376/2-1, the ERC project *EnSeNa* (257531) and the State of Bavaria. We thank A. Wolf and S. Kuhn for assistance during sample growth and fabrication.

---

[1] K. Edamatsu, “Entangled photons: Generation, observation, and characterization,” *Jpn. J. Appl. Phys.* **46**, 7175–7187 (2007).

[2] J.-W. Pan, Z.-B. Chen, C.-Y. Lu, H. Weinfurter, A. Zeilinger, and M. Zukowski, “Multiphoton entanglement and interferometry,” *Rev. Mod. Phys.* **84**, 777 (2012).

[3] O. Alibart, V. D’Auria, M. D. Micheli, F. Doutre, F. Kaiser, L. Labonte, T. Lunghi, E. Picholle, and S. Tanzilli, “Quantum photonics at telecom wavelengths based on lithium niobate waveguides,” *J. Opt.* **18**, 104001 (2016).

[4] Z. Y. Ou and L. Mandel, “Violation of bell’s inequality and classical probability in a two-photon correlation experiment,” *Phys. Rev. Lett.* **61**, 50 (1988).

[5] Y. H. Shih and C. O. Alley, “New type of einstein-podolsky-rosen-bohm experiment using pairs of light quanta produced by optical parametric down conversion,” *Phys. Rev. Lett.* **61**, 2921 (1988).

[6] P. G. Kwiat, K. Mattle, H. Weinfurter, A. Zeilinger, A. V. Sergienko, and Y. Shih, “New high-intensity source of polarization-entangled photon pairs,” *Phys. Rev. Lett.* **75**, 4337 (1995).

[7] Y.-K. Jiang and A. Tomita, “Highly efficient polarization-entangled photon source using periodically poled lithium niobate waveguides,” *Opt. Comm.* **267**, 278 (2006).

[8] H. C. Lim, A. Yoshizawa, H. Tsuchida, and K. Kikuchi, “Stable source of high quality telecom-band polarization-entangled photon-pairs based on a single, pulse-pumped,

short ppln waveguide,” Opt. Express **16**, 12460 (2008).

[9] T. Zhong, X. Hu, F. N. C. Wong, K. K. Berggren, T. D. Roberts, and P. Battle, “High-quality fiber-optic polarization entanglement distribution at 1.3  $\mu\text{m}$  telecom wavelength,” Opt. Lett. **35**, 1392–1394 (2010).

[10] A. Martin, A. Issautier, H. Herrmann, W. Sohler, D. B. Ostrowsky, O. Alibart, and S. Tanzilli, “A polarization entangled photon-pair source based on a type-ii ppln waveguide emitting at a telecom wavelength,” New J. Phys. **12**, 103005 (2010).

[11] H. Herrmann, X. Yang, A. Thomas, A. Poppe, W. Sohler, and C. Silberhorn, “Post-selection free, integrated optical source of non-degenerate, polarization entangled photon pairs,” Opt. Express **21**, 27981 (2013).

[12] A. Valles, M. Hendrych, J. Svozil, R. Machulka, P. Abolghasem, D. Kang, B. J. Bijlani, A. S. Helmy, and J. P. Torres, “Generation of polarization-entangled photon pairs in a bragg reflection waveguide,” Opt. Express **21**, 10841 (2013).

[13] A. Orieux, A. Eckstein, A. Lemaitre, P. Filloux, I. Favero, G. Leo, T. Coudreau, A. Keller, P. Milman, and S. Ducci, “Direct bell states generation on a iii-v semiconductor chip at room temperature,” Phys. Rev. Lett. **110**, 160502 (2013).

[14] R. T. Horn, P. Kolenderski, D. Kang, P. Abolghasem, C. Scarella, A. D. Frera, A. Tosi, L. G. Helt, S. V. Zhukovsky, J. E. Sipe, G. Weihs, A. S. Helmy, and T. Jennewein, “Inherent polarization entanglement generated from a monolithic semiconductor chip,” Sci. Rep. **3**, 2314 (2013).

[15] Z. H. Levine, J. Fan, J. Chen, and A. L. Migdall, “Polarization-entangled photon pairs from a periodically poled crystalline waveguide,” Opt. Express **19**, 6724 (2011).

[16] F. Kaiser, A. Issautier, L. A. Ngah, O. Danila, H. Herrmann, W. Sohler, A. Martin, and S. Tanzilli, “High-quality polarization entanglement state preparation and manipulation in standard telecommunication channels,” New J. Phys. **14**, 085015 (2012).

[17] N. Bruno, E. Z. Cruzeiro, A. Martin, and R. Thew, “Simple, pulsed, polarization entangled photon pair source,” Opt. Comm. **327**, 3 (2014).

[18] P. S. Kuo, T. Gerrits, V. B. Verma, and S. W. Nam, “Spectral correlation and interference in non-degenerate photon pairs at telecom wavelengths,” Opt. Lett. **41**, 5074–5077 (2016).

[19] F. Laudenbach, S. Kalista, M. Hentschel, P. Walther, and H. Hübel, “A novel single-crystal & single-pass source for polarisation- and colour-entangled photon pairs,” arXiv:1612.06579 (2016).

[20] D. Kang, M. Kim, and A. S. Helmy, “Two polarization-entangled sources from the same semiconductor chip,” Phys. Rev. A **92**, 013821 (2015).

[21] T. Günthner, B. Pressl, K. Laiho, J. Gessler, S. Höfling, M. Kamp, C. Schneider, and G. Weihs, “Broadband indistinguishability from bright parametric downconversion in a semiconductor waveguide,” J. Opt. **17**, 125201 (2015).

[22] D. Kang, A. Anirban, and A. S. Helmy, “Monolithic semiconductor chips as a source for broadband wavelength-multiplexed polarization entangled photons,” Opt. Express **24**, 15160 (2016).

[23] C. Autebert, J. Trapateau, A. Orieux, A. Lemaitre, C. Gomez-Carbonell, E. Diamanti, I. Zaquine, and S. Ducci, “Multi-user quantum key distribution with entangled photons from an algaas chip,” Quantum Sci. Technol. **1**, 01LT02 (2016).

[24] K. Laiho, B. Pressl, A. Schlager, H. Suchomel, M. Kamp, S. Höfling, C. Schneider, and G. Weihs, “Uncovering dispersion properties in semiconductor waveguides to study photon-pair generation,” Nanotechnology **27**, 434003 (2016).

[25] K. Mattle, H. Weinfurter, P. G. Kwiat, and A. Zeilinger, “Dense coding in experimental quantum communication,” Phys. Rev. Lett. **76**, 4656 (1996).

[26] L. Sansoni, F. Sciarrino, G. Vallone, P. Mataloni, A. Crespi, R. Ramponi, and R. Osellame, “Polarization entangled state measurement on a chip,” Phys. Rev. Lett. **105**, 200503 (2010).

[27] P. G. Kwiat, E. Waks, A. G. White, I. Appelbaum, and P. H. Eberhard, “Ultrabright source of polarization-entangled photons,” Phys. Rev. A **60**, R773 (1999).

[28] F. Steinlechner, P. Trojek, M. Jofre, H. Weier, D. Perez, T. Jennewein, R. Ursin, J. Rarity, M. W. Mitchell, J. P. Torres, H. Weinfurter, and V. Pruneri, “A high-brightness source of polarization-entangled photons optimized for applications in free space,” Opt. Express **20**, 9640 (2012).

[29] P. Chen, X. Guo, C. Shu, M. M. T. Loy, and S. Du, “Frequency-induced phase-tunable polarization-entangled narrowband biphotons,” Optica **2**, 505 (2015).

[30] W. P. Grice, A. B. U’Ren, and I. A. Walmsley, “Eliminating frequency and space-time correlations in multiphoton states,” Phys. Rev. A **64**, 063815 (2001).

[31] Y.-H. Kim and W. P. Grice, “Measurement of the spectral properties of the two-photon state generated via type ii spontaneous parametric downconversion,” Opt. Lett. **30**, 908 (2004).

[32] B. Pressl, T. Günthner, K. Laiho, J. Gessler, S. Höfling, M. Kamp, C. Schneider, and G. Weihs, “Mode-resolved fabry-perot experiment in low-loss bragg-reflection waveguides,” Opt. Express **23**, 33608 (2015).

[33] S. V. Zhukovsky, L. G. Helt, D. Kang, P. Abolghasem, A. S. Helmy, and J. E. Sipe, “Generation of maximally-polarization-entangled photons on a chip,” Phys. Rev. A **85**, 013838 (2012).

[34] B. Fang, O. Cohen, and V. O. Lorenz, “Polarization-entangled photon-pair generation in commercial-grade polarization-maintaining fiber,” J. Opt. Soc. Am. B **31**, 277–281 (2014).

[35] H.-T. Lim, K.-H. Hong, and Y.-H. Kim, “Effects of polarization mode dispersion on polarization-entangled photons generated via broadband pumped spontaneous parametric down-conversion,” Sci. Rep. **6**, 25846 (2016).

[36] D. F. V. James, P. G. Kwiat, W. J. Munro, and A. G. White, “Measurement of qubits,” Phys. Rev. A **64**, 052312 (2001).

[37] S. Hill and W. K. Wootters, “Entanglement of a pair of quantum bits,” Phys. Rev. Lett. **78**, 5022 (1997).